

PAPER • OPEN ACCESS

## Triply periodic minimal surfaces based functionally graded biomimetic scaffold fabrication via stereolithography

To cite this article: Y W Adugna *et al* 2023 *IOP Conf. Ser.: Mater. Sci. Eng.* **1294** 012051

View the [article online](#) for updates and enhancements.

You may also like

- [Surface curvature in triply-periodic minimal surface architectures as a distinct design parameter in preparing advanced tissue engineering scaffolds](#)  
Sébastien B G Blanquer, Maike Werner, Markus Hannula et al.
- [3D printing polyurethane acrylate\(PUA\) based elastomer and its mechanical behavior](#)  
Huan Li, Lei Liang, Wenxiang Zeng et al.
- [3D printed flexible wearable sensors based on triply periodic minimal surface structures for biomonitoring applications](#)  
Mohammad Ebrahim Imanian, Mostafa Kardan-Halvaei, Fatemeh Nasrollahi et al.

**PRIME**  
PACIFIC RIM MEETING  
ON ELECTROCHEMICAL  
AND SOLID STATE SCIENCE




HONOLULU, HI  
Oct 6-11, 2024

Abstract submission deadline:  
**April 12, 2024**

Learn more and submit!

**Joint Meeting of**  
The Electrochemical Society  
•  
The Electrochemical Society of Japan  
•  
Korea Electrochemical Society

# Triply periodic minimal surfaces based functionally graded biomimetic scaffold fabrication via stereolithography

Y W Adugna<sup>1,\*</sup> , H G Lemu<sup>1</sup>  and H R Hagland<sup>2</sup> 

<sup>1</sup> Department of Mechanical and Structural Engineering and Materials Science, University of Stavanger, Stavanger, Norway

<sup>2</sup> Department of Chemistry, Biosciences and Environmental Engineering, University of Stavanger, Stavanger, Norway

\* Correspondence: yosef.w.adugna@uis.no

**Abstract.** Triply Periodic Minimal Surfaces (TPMS), a class of intricate mathematical surfaces, have emerged as a promising framework for scaffold design due to their ability to replicate the complex geometries found in biological structures. Four TPMS structures, the Schwarz Diamond (D), Schwarz Primitive (P), Gyroid, and IWP (I-wrapped package) were designed for both uniform and graded density and additively manufactured through Stereolithography based additive manufacturing (AM) techniques using biomedical graded material. Two different mechanical tests, tensile and compression tests were examined on the TPMS structure to study their mechanical properties. The results showed that Schwarz D and IWP TPMS show greater tensile strength for both uniform and graded structures with 18.22 MPa and 14.41 MPa in uniform structures and 9.89 MPa and 9.23 MPa in graded structures of Schwarz D and IWP respectively. Uniform TPMSs show overall tensile strength over the graded TPMS. Compressive properties also show that Schwarz D and IWP TPMS have greater compressive strength in both uniform and graded TPMS, where overall graded structures show better strength over the uniform. Graded Schwarz D observed to have 100.68 MPa, and IWP TPMS has 99.57 MPa, and uniform Schwarz D has 33.94 MPa, whereas IWP TPMS shows 31.82 MPa compressive strength. Results reinforce the structure's suitability for scaffold applications, particularly in contexts demanding robust mechanical integrity. The application of SLA AM with biomedical-graded material strengthens the viability in areas like tissue engineering and regenerative medicine.

**Keywords:** Triple periodic minimal surface (TPMS), Tissue engineering, Biomimetic, Stress-strain curve

## 1. Introduction

Bone tissue engineering (BTE) is in great demand for the repair of defective bones due to an aging population and the increasing use of high-speed transportation, both of which are associated with an increase in bone diseases [1]. Diseased or injured bone tissue presents a significant requirement for bone replacements used in transplantation, making it the second most often transplanted tissue on an annual basis [2]. Access to bone replacements is a challenge and has been an area under intense research to find a solution to solve this issue, where Langer and Vacanti's 1993 Science article describing the properties and applications of biodegradable 3D scaffolds was pivotal in the development of the new field - tissue engineering [3].



The primary objective of tissue engineering is to imitate the inherent characteristics of natural tissue by facilitating tissue regeneration through the integration of a scaffold, cells, and bioactive molecules. One prominent benefit of bone tissue is its inherent capacity for self-repair, remodelling, and regeneration. Consequently, bone tissue engineering holds promise as a potential approach for addressing bone defects resulting from diverse causes [4].

The internal biological structure of bone tissue is characterized by a complex, porous, and curved composition, featuring irregular pore structure and uneven pore size and distribution. Additionally, the presence of internal communication pores facilitates the transportation of nutrients from the external environment to the interior of the system [5]. Presently, orthopedic implants like bone nails, bone plates, and intramedullary nails are not customized to match the specific bone characteristics of individual patients. Consequently, this lack of tailoring contributes to an elevated occurrence of complications during surgical procedures [6]. Furthermore, the presence of a significant mismatch in modulus between the bone and the implant results in stress shielding, which occurs because of the non-uniform distribution of stress at the interface between the bone and the implant. Thus, cellular materials are used to customize the characteristics of the implant and mitigate bone resorption around the implant caused by the stress shielding phenomenon [7].

Lattices represent a compelling subset of cellular materials and find extensive use in the design of body implants and scaffolds [8]. Triply periodic minimum surfaces (TPMS) are minimally shell-based sized surfaces with closed curves as boundaries, defined mathematically [9]. These surfaces serve as the foundation for TPMS scaffolds. Each unit cell is created by adding thickness to the surface, and the finished scaffold is cubically symmetric and has periodic repetitions of connected pores [10]. As an essential type of porous structure, functionally graded structures are an ideal option for producing lightweight, stress-resistant, and high-energy-absorbing components, which is also one of the reasons TPMS structures have attracted attention [11].

The design and pore geometry of scaffolds plays a significant role in the organization of cells and tissues in tissue-engineered constructs. The high biological and functional complexity of human tissues with specific micro-architecture and vascular networks require the use of more specific scaffold geometries made from multifunctional materials and structures [12]. Ideal 3D scaffolds should be highly porous, have interconnected pore networks, and have pores of a consistent and sufficient size for cell infiltration and migration [13]. As such, controlling porosity, pore size, surface area, and permeability, as well as manipulating strength and stiffness, is essential [14]. In general, a scaffold should provide a microenvironment that stimulates cell growth through cell-scaffold and cell-cell interactions, such as adhesion, differentiation, proliferation, migration, and maintenance [15, 16].

The formation of a porous structure inside the scaffold is one of the important elements in the manufacture of tissue engineering scaffolds both for uniform and graded structures [17]. Various conventional manufacturing techniques have been utilized to fabricate porous 3D scaffolds, such as solvent casting, fiber bonding, particulate leaching, phase separation membrane lamination, foaming, and moulding [18]. However, a limitation of all these approaches is the insufficient control over scaffold design, pore network, and pore size, resulting in the production of inconsistent and inefficient three-dimensional scaffolds [19]. Moreover, most of the traditional implants are solid structures, and their mechanical properties are unsatisfactory for the adjacent bone tissues, resulting in the occurrence of stress shielding between them [6]. On the other hand, the ongoing development of Additive manufacturing (AM) technology provides a promising method for fabricating structures with complex external geometries and well-defined internal connections i.e., in the creation of customized porous scaffolds [20].

Regardless of the material used, different AM technologies are employed to manufacture porous structures including selective laser melting (SLM), selective laser sintering (SLS), fused deposition modelling (FDM), digital light processing (DLP), stereo lithography apparatus (SLA) and others [21-25]. Most of the previous research preferred SLS and SLM. SLA AM technology is known for its efficiency, high dimensional accuracy, and speed. It offers unique ways to accurately control substrate architecture [26, 27]. Some of the studies on TPMS scaffolds manufactured through SLA, including Yu.

et. al., investigated the mechanical properties and energy absorption abilities of Schwarz P and Gyroid TPMS structures manufactured through SLA [28]. Chouhan *et. al* studied surface defects of Gyroid TPMS through varied thicknesses produced with SLA [29].

Previous investigations on TPMS have mainly focused on metallic additive fabrication, and the number of studies on SLA-manufactured TPMS structures is limited. In this work, four (4) different uniform and functionally graded TPMS structures (Schwarz P, Schwarz D, Gyroid, and IWP) were designed and fabricated by using the SLA AM technique, and their mechanical property is examined. A smooth variation in density was achieved in the graded TPMS structures by distributing the wall thickness linearly and continuously. The accuracy and manufacturability of SLA-fabricated TPMS specimens are investigated. Mechanical properties of both uniform and graded structures were examined through tensile and compression tests.

## 2. Materials and methods

### 2.1 Material

In this work, a medical-grade photocurable vat photopolymerization resin from Formlabs (Formlabs Inc., Somerville, MA, USA - Biomed Clear Resin (Product Code: FLBMCL01)) is used. BioMed clear resin is a photopolymer resin made of a mixture of methacrylic esters and photoinitiators. It is a light-curable polymer-based material designed for AM of medical grade, biocompatible, clear, and rigid parts for long-term surface contact. Table 1 and Table 2 provide Biomed clear material composition and properties according to the manufacturer's data [30].

**Table 1.** Biomed clear material composition

Material	Concentration, (wt.%)
Bisphenol A dimethacrylate	~50–70
2-hydroxyethyl methacrylate monomer(s)	7–10
Urethane dimethacrylate	25–45
Photoinitiator(s)	< 2

**Table 2.** Biomed clear properties

Material	Density, (g/cm <sup>3</sup> )	Ultimate tensile strength (MPa)	Young's Modulus, (MPa)	Elongation (%)	Hardness, (Shore - D)
Biomed clear	1.09	52	2080	12	78

### 2.2. Structure design of TPMS

The Computer-Aided Design software Creo® Parametric (TM)<sup>TM</sup>, based in Boston, MA, USA, was utilized to generate macro-lattice designs. The lattice tool of Creo® Parametric (TM) was utilized to generate various unit cells within part files. Subsequently, cell arrangements were formed from these part files and merged into part files to construct the overall intended structures. Mathematical representations of the surfaces are as follows:

$$(i) \text{ Diamond: } \cos(\omega x) \cos(\omega y) \cos(\omega z) - \sin(\omega x) \sin(\omega y) \sin(\omega z) = c. \quad (1)$$

$$(ii) \text{ Primitive: } \cos(\omega x) + \cos(\omega y) + \cos(\omega z) = c. \quad (2)$$

$$(iii) \text{ Gyroid: } \cos(\omega x) \sin(\omega y) + \cos(\omega y) \sin(\omega z) + \cos(\omega z) \sin(\omega x) = c. \quad (3)$$

$$(iv) \text{ IWP: } 2[\cos(\omega x) \cos(\omega y) + \cos(\omega y) \cos(\omega z) + \cos(\omega z) \cos(\omega x)] - [\cos(2\omega x) + \cos(2\omega y) + \cos(2\omega z)] = c. \quad (4)$$

Where,  $\omega$  is used to define the unit cell length, and  $c$  controls the expansion of the surface in three dimensions. The unit cell design of the generated TPMS structure, constructed  $3 \times 3 \times 3$ , is seen in Figure 1.

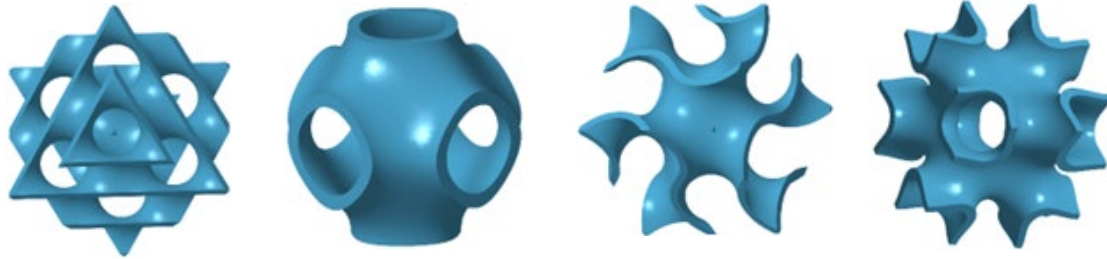


**Figure 1.** Unit cell design of TPMS structures (a) Schwarz D, (b) Schwarz P, (c) Gyroid and (d) IWP

For the tensile test specimen, the gauge length area of the specimen is considered for the generation of the TPMS structure. Whereas for the compression test, the whole geometry is considered. The lattices were constructed through repeating the unit cells through the part geometry. The uniform structure was designed to have a wall thickness of 0.3. The graded structure was built with a linear and continuous variation in wall thickness, ranging from 0.2 to 0.5 mm in the building's direction during the SLA printing process. Designed CAD models of the tensile and compression specimens are seen in Figure 2 and Figure 3, respectively.

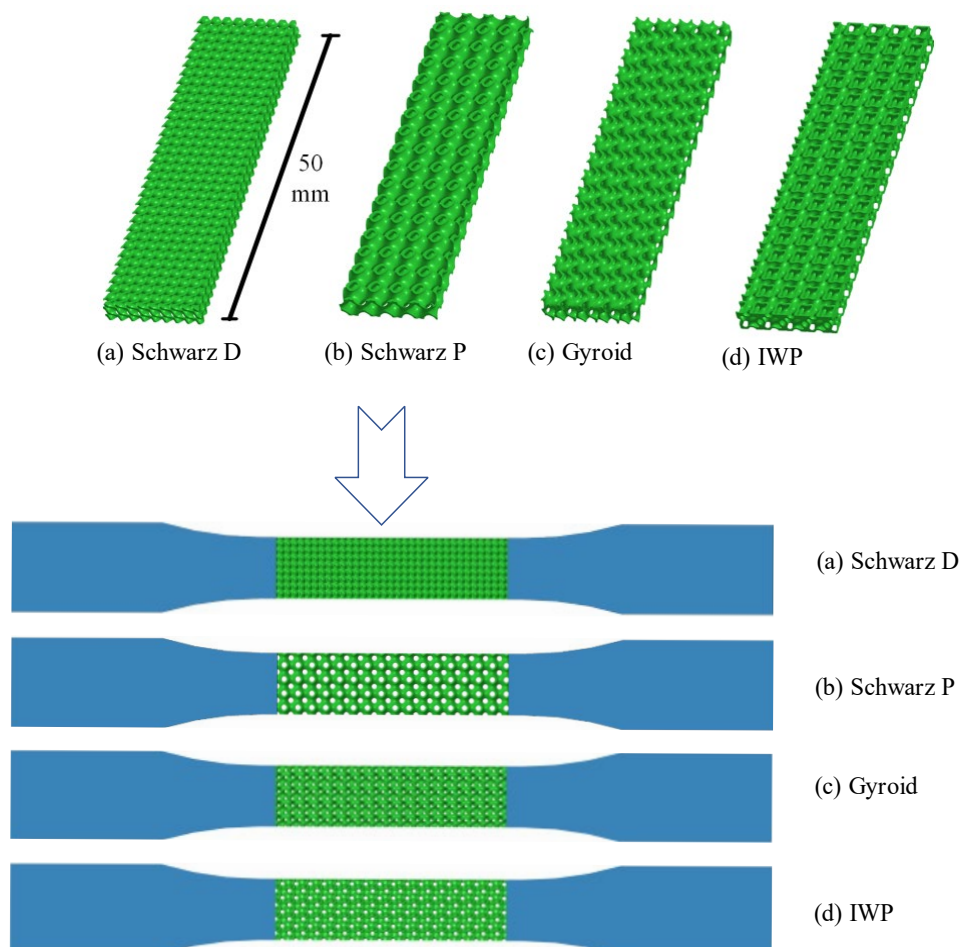


**Figure 2.** CAD Designed tensile specimen with TPMS generated at gauge length

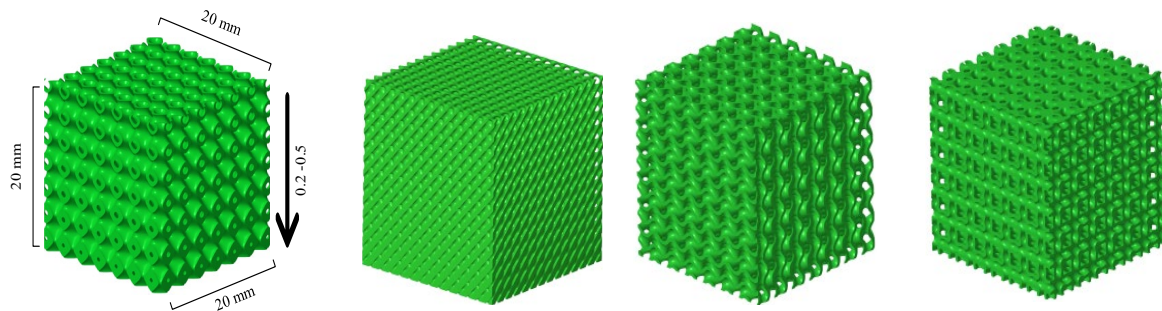


**Figure 3.** CAD-designed models of compression test specimens.

### 2.3. SLA 3D Printing

The 3D printer used was a Formlabs Form 3B+ (Formlabs Ohio Inc., Millbury, OH, USA) vat photopolymerization 3D printer with Formlabs Tank LT. The preparation of the necessary GCode and the slicing process was implemented on the Preform 3.16 software tool. Biomed Clear resin was 3D printed with 100  $\mu\text{m}$  layer height for every case tested. The specimens were additively manufactured with a horizontal orientation on the build plate. After the 3D-printing process was completed, specimens were washed in a 99% pure isopropyl alcohol (IPA) solution for 15 min and dried for 5 min at room temperature and ambient conditions (this method was repeated twice), according to Formlabs specifications and guidelines. When the IPA cleaning process of the specimens was completed, a post-curing period of 60 min at 60  $^{\circ}\text{C}$  took place. Formlabs Form Wash and Form Cure (Formlabs Ohio Inc., Millbury, OH, USA) equipment have been used for the washing and the post-curing processes, respectively. Form 3B+ is equipped with a 405 nm UV laser. Three duplicates of each specimen type are manufactured for testing.

**Table 3.** SLA 3D Printing parameter

Parameter	Value
Slicing software	Preform v3.29
Layer height	100 $\mu\text{m}$
Build orientation	45 $^{\circ}$
Wash time	15 min (99% IPA)
Dry time	5 min (99% IPA)

### 2.4. Mechanical testing

The tensile test specimen is prepared according to the ASTM D638 type IV standard. ASTM D638 type IV has a 50 mm gauge length. Thus, the total length of the gauge length (50 mm) is used for the generation of different TPMS structures. The tensile properties of additive manufactured tensile test specimens with TPMS structure were tested using Instron tensile testing machine that has a load cell capacity of 10 kN, at a speed of 2 mm/min, and a sampling frequency of 50 hz.

Compression test specimen is prepared according to the standard ASTM D-695. The initial design of the specimen has a cubic geometry with the dimensions of 20 x 20 x 20  $\text{mm}^3$ . The Instron tensile testing machine with a load cell of 250 kN is used for a compression test. The test was set to terminate when the nominal strain reached 70% of the specimen geometry (14mm) and specimen fracture, respectively.

### 3. Results and discussion

#### 3.1. Tensile test result

Before the production of specimens, it is crucial to consider a significant aspect in the context of the tensile test specimen, namely the occurrence of stress concentration at the solid-lattice transition, and failure near the grip section due to non-uniform stress at the interface. The presence of stress concentration resulting from the abrupt cross-sectional variation in the solid-lattice transition zone, which is deemed insignificant in the context of the compression test, can give rise to premature fracture of the components subjected to tensile loading, hence compromising the reliability of the test results. In the first design, the TPMS structure has a sudden change of cross section from porous to solid, but this clearly shows where the failure might happen. In the second design, grading of the transition between TPMS and the solid interface is introduced which significantly prevents the stress concentration, it was hypothesized that the lattices may be gradually graded as they make the transition into the solid zone, resulting in an augmented cross-sectional area of the material inside the region. The first design failed, and the specimens were manufactured using the second option. The designed specimens were successfully manufactured using the SLA AM technology. Figure 4 displays the as-manufactured tensile test specimen and the after-test broken specimen.

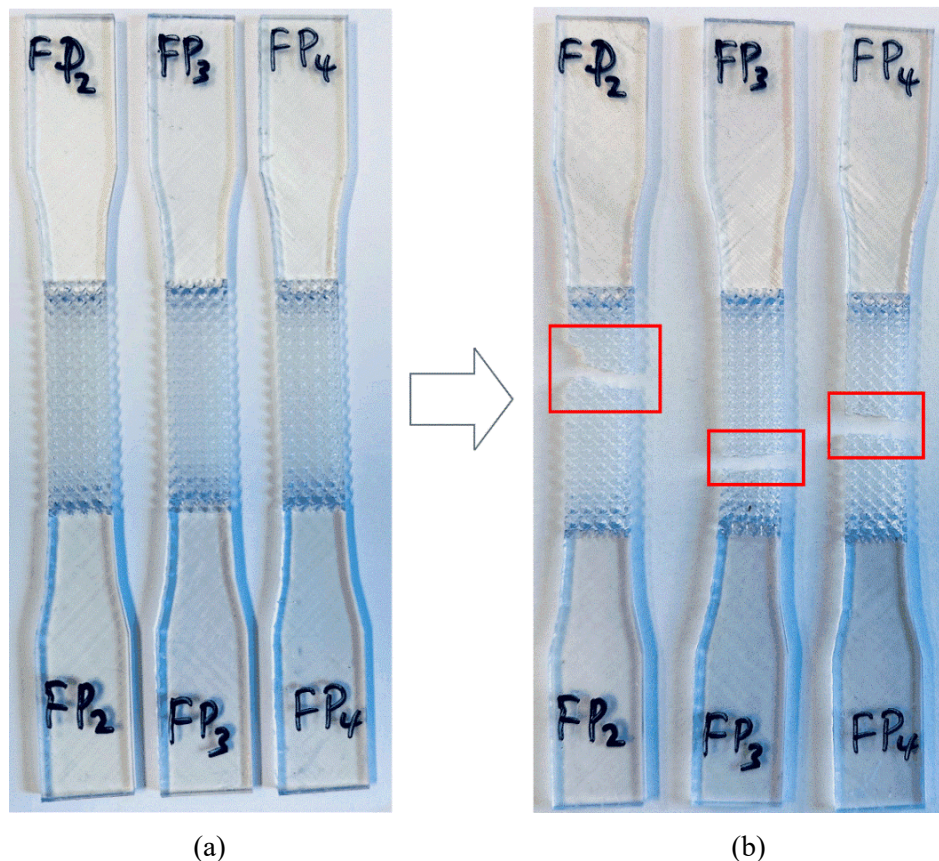
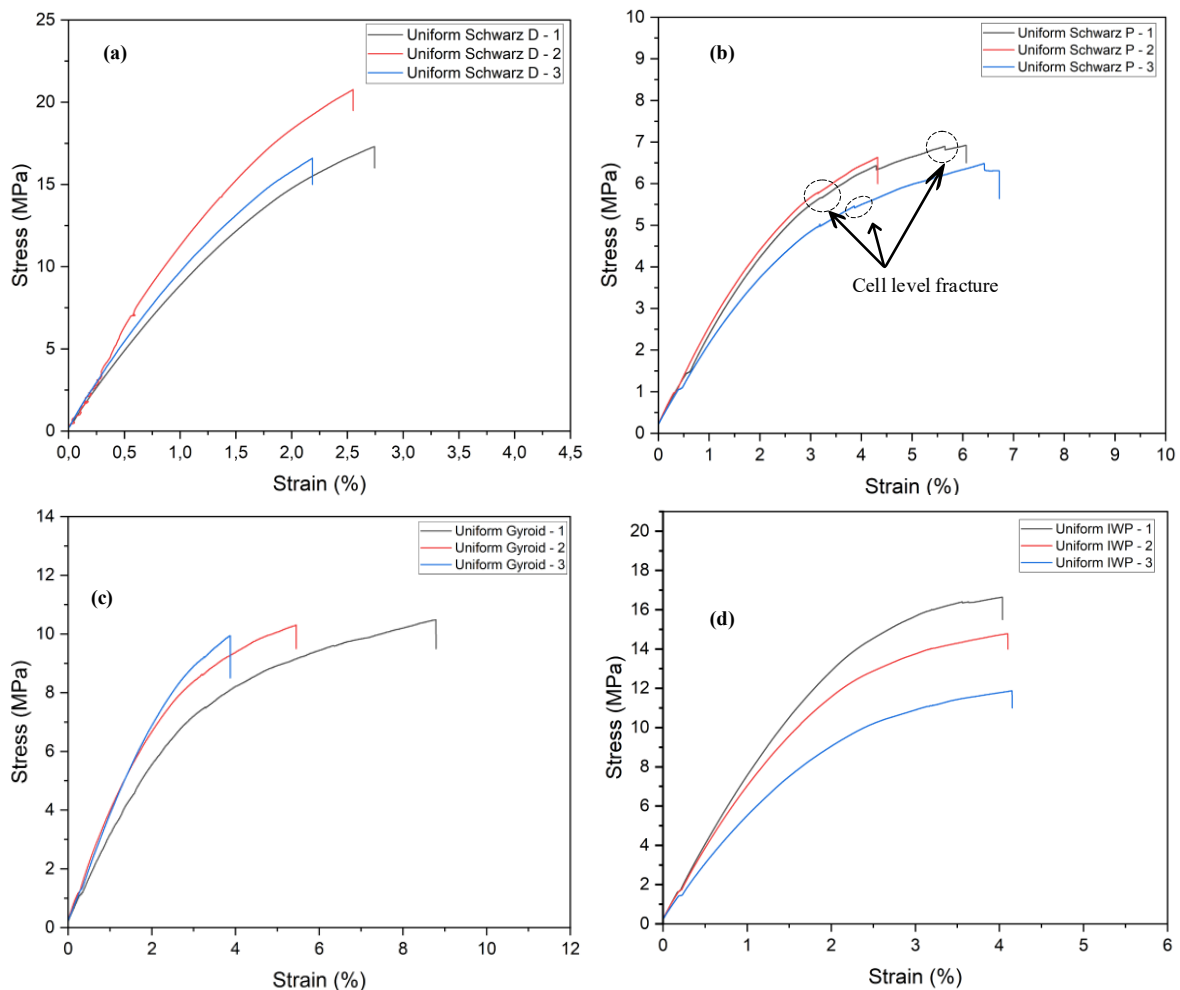


Figure 4. Specimen label (a) and After test specimen (b)

The tensile stress-strain curve for the AM'ed Uniform TPMSs is presented in Figure 5. The tensile response of some of the uniform TPMS constructions consists of a linear elastic zone, which is then followed by strain hardening in the same manner as the solid specimens i.e., Schwarz P and IWP TPMS. Whereas Schwarz D and Gyroid show fracture before reaching the strain hardening zone. An observable phenomenon characterized by a step-like pattern in stress decrease is evident before the occurrence of

ultimate fracture, suggesting the occurrence of failure at the level of cells inside the TPMS structures. This can be seen clearly on the Uniform Schwarz P stress-strain curve (Figure 5b).

Schwarz D TPMS shows the highest mean tensile strength of 18.22 MPa, suggesting higher structural integrity and superior resistance to deformation under the applied tensile forces. IWP TPMS follows with a mean tensile strength of 14.41 MPa, showing substantial capacity to withstand loads. The intermediate level of strength could be attributed to the inherent geometric features and interconnectivity within the IWP structure. The Schwarz P shows the lower mean tensile strength, 6.67 MPa among all uniform TPMS structures.



**Figure 5.** Stress-strain curve of Uniform TPMS Tensile test (a) Schwarz D (b) Schwarz P (c) Gyroid (d) IWP

All Uniform TPMS structures showed ductile behaviour during testing. Gyroid TPMS exhibited the highest mean elongation, reaching 3.7%. Next to Gyroid TPMS is Schwarz P. TPMS failed at 2.53% of mean elongation. Schwarz D TPMS is the lowest of all uniform TPMS with 0.89% mean elongation. It is noteworthy to mention that the observed reduction in elongation might be ascribed to the curing process that the material undergoes after production. In addition to the materials removed to generate the TPMS structure, the observed decrease in elongation can be attributed to the structural modifications that take place during the curing process.

The individual TPMS tensile stress-strain curve of the four Graded TPMS structures is given in Figure 6. Comparing the tensile strength of the graded TPMS structure, most of them show similarity



except Gyroid. Schwarz D and IWP show closer highest tensile strength at 9.9 MPa and 9.22 MPa respectively whereas Schwarz P follows with 7.38 MPa of mean tensile strength. Gyroid demonstrates a comparatively lower mean tensile strength with 4.05 MPa compared to other graded TPMS structures.

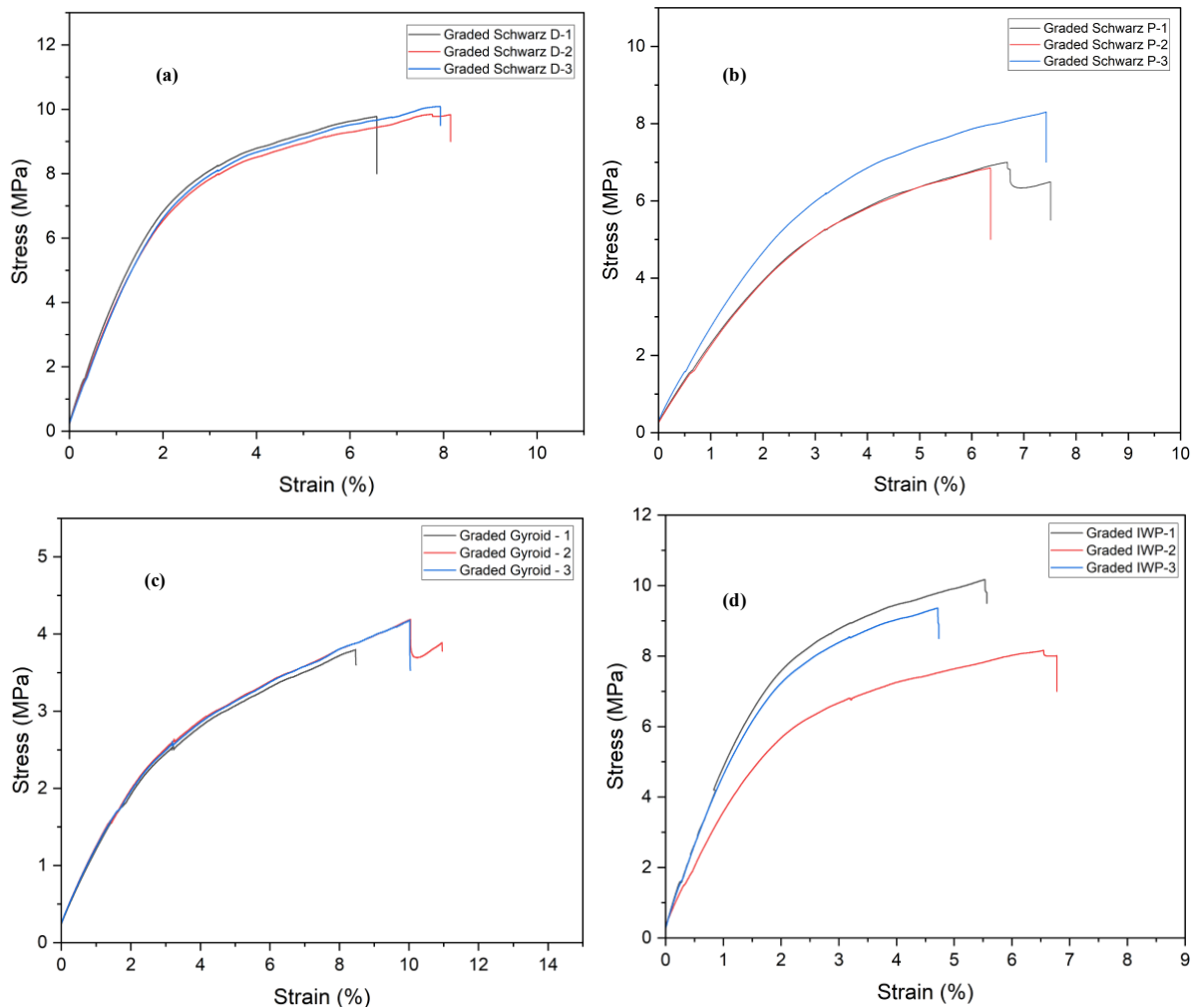


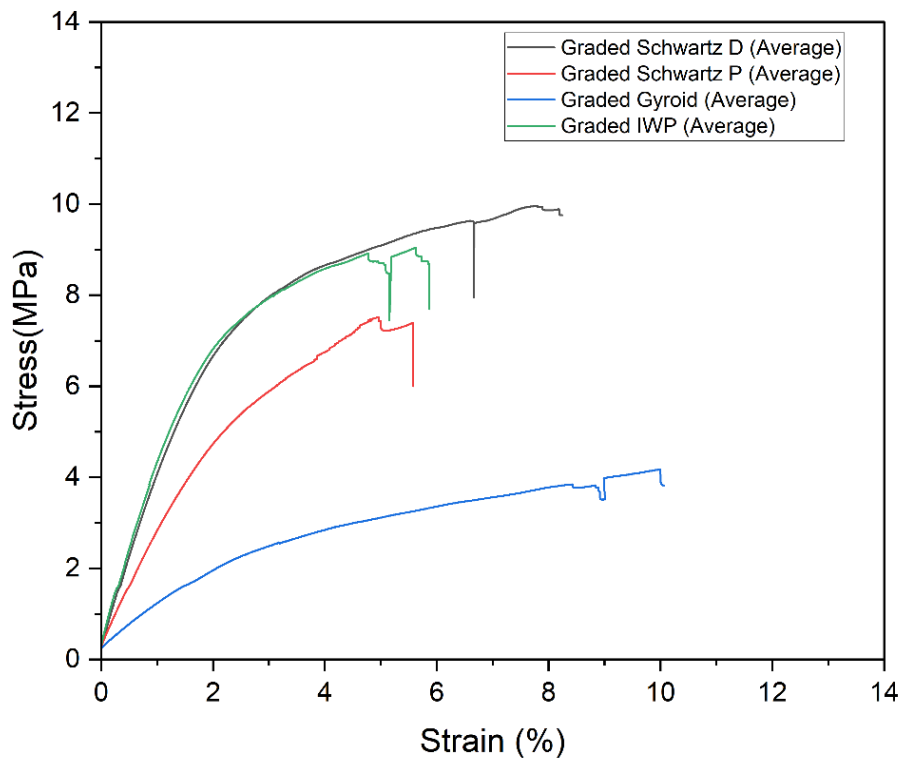
**Figure 6.** Stress-strain curve of Graded TPMS Tensile test (a) Schwarz D (b) Schwarz P (c) Gyroid (d) IWP

The graded TPMS constructions, much like the uniform structures, demonstrated ductile behaviour. Among all the Gyroid TPMS had the highest level of resilience against deformation, and greatest elongation, reaching 5.6%. The Schwarz D TPMS structure exhibited a significant elongation of 4.9%, in close succession. This observation implies a notable capacity for undergoing deformation while concurrently preserving structural integrity. Schwarz P and IWP TPMS structures had comparatively lower elongations, measured at 3.5% and 3.4% respectively. Although the ductility of these values is significantly lower in comparison to Gyroid and Schwarz D, they nonetheless fall within the acceptable range of mechanical performance for several applications. In contrast, the structures of Schwarz P and IWP TPMS exhibited comparatively lower mean elongations, measured at 3.5% and 3.4% respectively. The comparative results from the tensile properties of the uniform and graded TPMSs are summarized in Table 4 and Figure 7.

**Table 4.** Summarized tensile property of uniform and graded TPMS

TPMS geometry	Wall thickness (mm)	Max. Force (kN)	Tensile strength (MPa)	Elongation (%)	Elastic modulus (MPa)
Schwarz D	Uniform	0.3	758	18.22	0.89
	Graded	0.2 - 0.5	412	9.89	4.8
Schwarz P	Uniform	0.3	278	6.68	2.5
	Graded	0.2-0.5	307	7.38	3.5
Gyroid	Uniform	0.3	426.3	10.25	3.74
	Graded	0.2-0.5	161	4.05	5.6
IWP	Uniform	0.3	597	14.41	1.9
	Graded	0.2-0.5	383.6	9.23	3.4

The comparative tensile stress-strain curve of all structures, both uniform and graded TPMS considered for this study is seen in Figure 7. In both cases, Schwarz D TPMS shows greater mean tensile strength. The mean tensile strength of graded Schwarz D TPMS (18.22 MPa) is close to double for uniform Schwarz D (9.9 MPa). Schwarz P exhibits relevant mean tensile strength in both cases, where the graded tensile strength (7.39 MPa) is higher than the uniform (6.67 MPa). This implies that the graded structure enhances the tensile strength of Schwarz P TPMS. The mean tensile strength of uniform Gyroid TPMS is more than double (10.25 MPa) to the mean tensile strength of graded Gyroid TPMS (4.05 MPa). A similar trend is observed in IWP, the uniform shows the highest mean tensile strength (14.41 MPa) than graded TPMS (9.23 MPa). This further supports the trend observed across the other TPMS structures, where uniform structures tend to yield greater mean tensile strength.

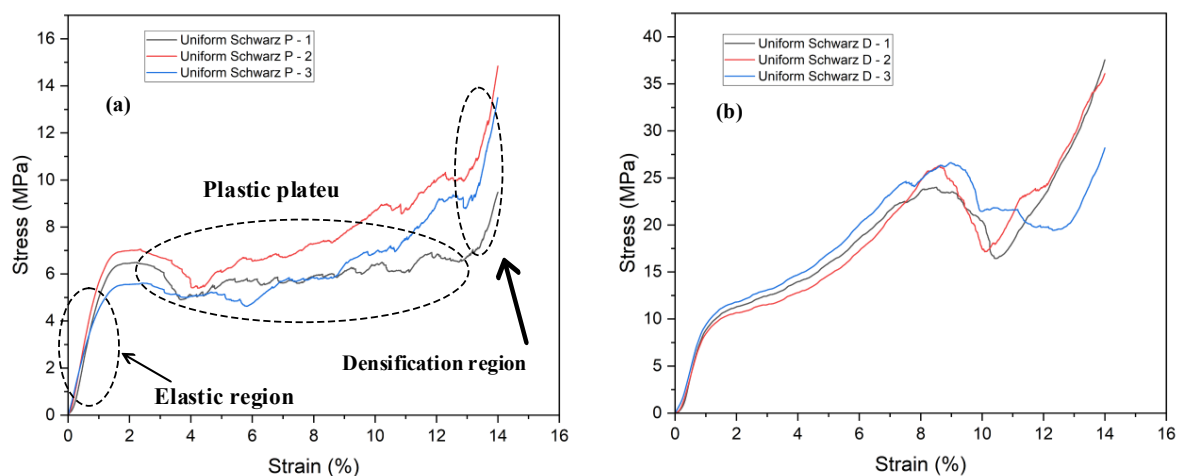
**Figure 7.** Stress-strain curve of TPMS structures under tension

In all of them, uniform TPMS structures show greater mean tensile strength except Schwarz P where the graded TPMS is higher. The observed variations in mean tensile strength among different TPMS structures can be attributed to their unique geometric properties and compositions. Uniform TPMS structures tend to exhibit higher tensile strength in most cases, as they maintain a consistent material distribution and are less prone to stress concentration. The variation in thickness results in variation of stress and material distribution in a graded TPMS can be considered as the major factor for comparatively less strength.

The analysis of ductility among the structures reveals compelling insights into their mechanical behaviour highlighting graded TPMS's superior elongation properties compared to their uniform counterparts. The graded Schwarz D TPMS displays a remarkable mean elongation of 4.87%, indicating its substantial capacity to undergo plastic deformation before failure. In contrast, the uniform Schwarz D TPMS exhibits a significantly lower mean elongation of 0.89%. This difference can be attributed to the change in the cross-section area of the graded TPMS which allows more elongation under stress. In Schwarz P TPMS a similar trend is observed. The graded Schwarz P TPMS shows a notable mean elongation of 3.5%, indicating its ability to undergo plastic deformation before failing. On the other hand, the uniform Schwarz P TPMS exhibits a slightly lower mean elongation of 2.53%. The graded Gyroid TPMS exhibits a substantial mean elongation of 5.6%. In contrast, the uniform Gyroid TPMS achieves a mean elongation of 3.75%, which, while still notable, falls short of the uniform structure's ductility. In the case of IWP TPMS, the graded structure displays a mean elongation of 3.4%, highlighting its capacity for plastic deformation. On the other hand, the uniform IWP TPMS exhibits a lower mean elongation of 1.9%. The observed increase in ductility in graded TPMS structures compared to uniform ones can be attributed to the graded structure's capacity to distribute stresses and strains more effectively. This leads to a higher degree of deformation before structural failure.

### 3.2. Compression test result

Compression results of tested TPMS structures are provided in Figure 8, Figure 9, and Table 5. Stress-strain curves for a typical lattice structure display three different regions: (1) an elastic compression region, where the stress rises linearly with strain during the elastic stage, illustrating a linear stress-strain relationship; (2) a plateau region following the elastic region, which is marked by a reduction in stress and load-carrying capacity because of wall yield, plastic deformation, buckling, and fracture of the lattice walls; and (3) a densification region, where collapsed walls and cells come into contact and cause a significant increase in stress [31].



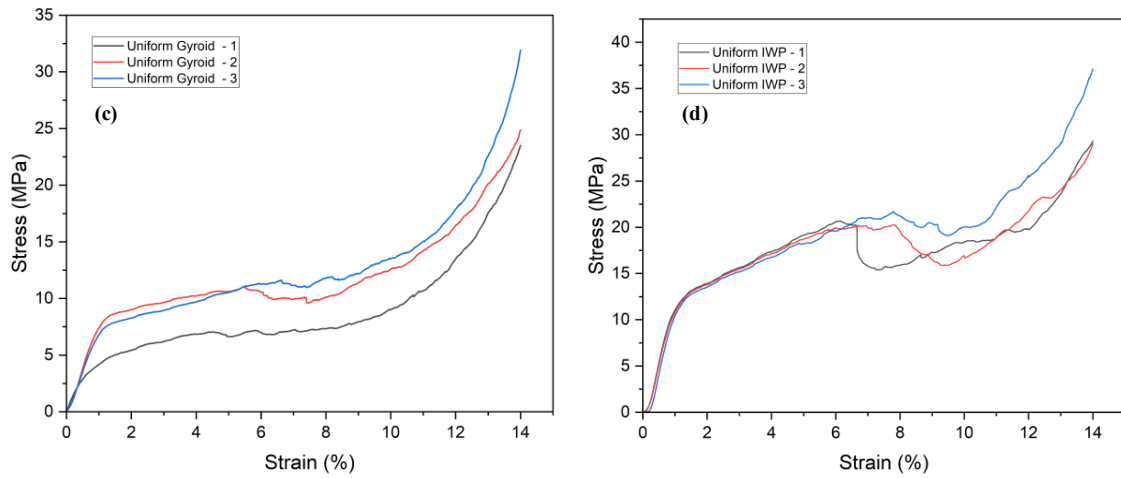


**Figure 8.** Stress-strain curve of uniform TPMS under compression (a) Schwarz D (b) Schwarz P (c) Gyroid (d) IWP

Figure 8 above displays the stress-strain property of uniform TPMS of Schwarz D, Schwarz P, Gyroid, and IWP where the elastic, plastic deformation and densification regions can be seen clearly. All four uniform structures exhibit elastic properties at lower strains. This is a characteristic common to many materials, wherein at low levels of stress, the material can deform elastically and return to its original shape once the stress is removed. This behavior is typically governed by the material's elastic modulus, which reflects its stiffness. As shown in the uniform Schwarz P stress-strain curve, the plastic collapse happened when the structure reached the first peak of the stress. Schwarz D demonstrates the highest mean compressive strength with 33.94 MPa, and IWP TPMS also closer with 31.82 MPa. This suggests that IWP TPMS is similarly adept at withstanding compressive loads. Gyroid has 26.78 MPa and Schwarz P with the lowest compressive strength 12.6 MPa. Schwarz P exhibits repeating ups and downs in the stress-strain curve, an indication of a layer-by-layer deformation pattern. It can be considered as every up and down attribute to each layer cell row deformation. Schwarz D, Gyroid, and IWP TPMS's stress-strain curve shows the structures deformed uniformly, an indication of consistent load bearing. The deformation behavior of the structures in the densification region is much like those of the solid parts and exhibits fast stress increment.

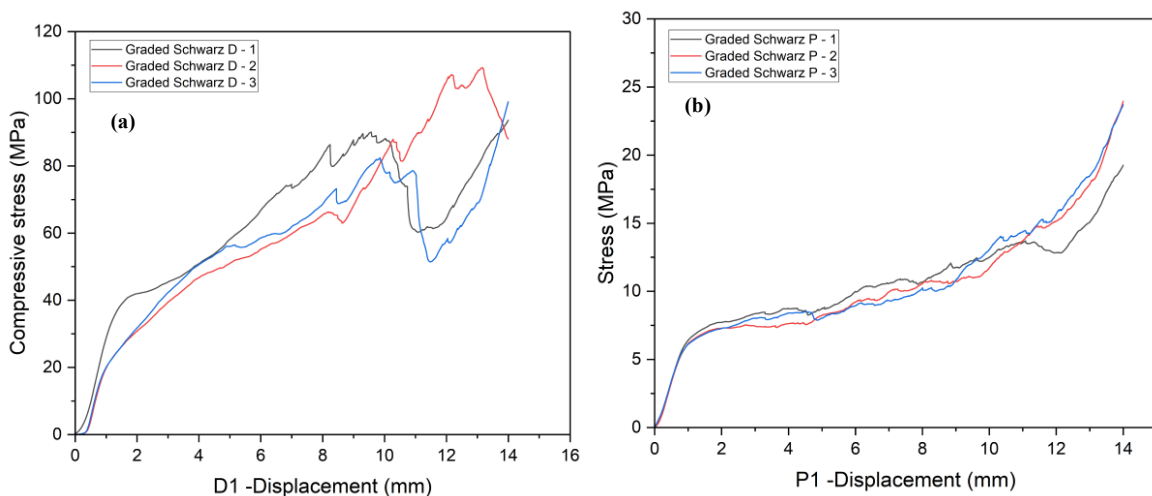


**Figure 9.** Stress-strain curve of Graded TPMS under compression (a) Schwarz D (b) Schwarz P (c) Gyroid (d) IWP

The graded TPMS structures stress-strain curve under compression is seen in Figure 9. Graded structures show overall greater compressive strength compared to the uniform TPMS. Schwarz D exhibits 100.68 MPa. The geometric arrangement and composition of Schwarz D in its graded form play a crucial role in achieving this high compressive strength. Like the uniform pattern, graded IWP TPMS also exhibits close mean compressive strength to the Schwarz D with 99.57 MPa. The fact that it approaches the performance of Schwarz D suggests that IWP when graded, can be a viable alternative for applications requiring high compressive strength. The Gyroid shows a mean compressive strength of 46.39 MPa. Whereas the Schwarz P has a comparatively lower mean strength of 22.3 MPa under compression. The summary of the different mechanical properties of both uniform and graded TPMS structures can be found in Table 5.

**Table 5.** Mechanical properties of Schwartz D, Schwarz P, Gyroid, and IWP TPMS Structures under compression

TPMS		Wall thickness (mm)	Max. Force (kN)	Compressive strength (MPa)	Compressive modulus (MPa)
Schwarz D	Uniform	0.3	13.58	33.94	233.98
	Graded	0.2 - 0.5	40.27	100.68	738.28
Schwarz P	Uniform	0.3	5.04	12.6	128
	Graded	0.2-0.5	8.92	22.3	171.7
Gyroid	Uniform	0.3	10.71	26.78	185.56
	Graded	0.2-0.5	18.56	46.39	194.08
IWP	Uniform	0.3	12.73	31.82	313.72
	Graded	0.2-0.5	39.83	99.57	684.97

Figure 10 shows the overall stress-strain curve under compression test for both uniform and graded TPMS structures. The compressive strength shows great variability between the two cases. The trend in both cases follows the same pattern in terms of highest to lowest mean strength. Schwarz D TPMS, whether graded or uniform, exhibits the highest mean compressive strength. Schwarz D's graded mean compressive strength (100 MPa) and IWP TPMS's graded mean compressive (99.47) are 3 times the strength in uniform of their respective (33.94 MPa for Schwarz D and 31.82 MPa for IWP). Schwarz P's graded mean compressive (22.3 MPa) is close to twice the strength exhibited in uniform (12.6 MPa). The Graded Gyroid (46.39) also displays greater mean strength to the uniform (26.78 MPa)

Overall grading of the TPMS structure according to their function enhances their compressive strength. These highlight the potential of graded TPMS materials for applications where high compressive strength is a critical requirement, such as in structural components subjected to heavy loads or in orthopaedic implants.

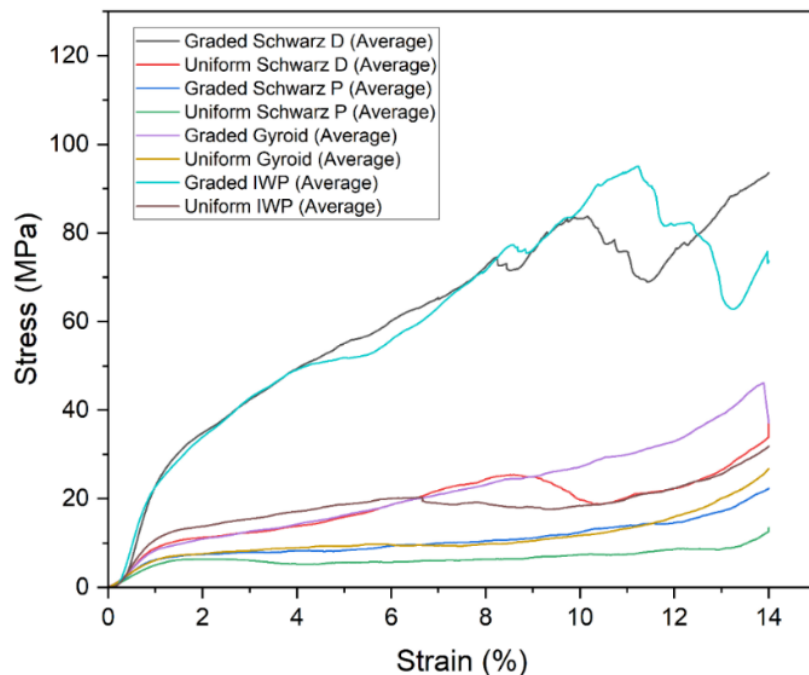


**Figure 10.** Stress-strain curve of TPMS structures under compression.

#### 4. Conclusion

In this study, uniform and functionally graded four TPMS structures namely Schwarz Diamond (D), Schwarz Primitive (P), Gyroid and IWP were designed and successfully manufactured through SLA AM technology. The SLA AM technology proved to be highly effective in manufacturing complex structures with a good surface finish and accuracy. The mechanical properties of the structures were analyzed through tensile and compressive tests on the manufactured specimens. It is notable that both uniform and graded Schwarz D TPMS structures exhibited greater mean tensile strength compared to the other structures. Both uniform and graded Schwarz D TPMS show greater mean tensile strength, also greater compressive strength in both cases of uniform 18.22 MPa and graded structures with 9.89 MPa structures. IWP follows in tensile strength observed to have 14.41 MPa in uniform structure whereas the graded structure has 9.23 MPa. Additionally, both Schwarz D and IWP TPMS displayed higher compressive strength across all tests in both uniform and graded cases. Graded Schwarz D observed to have 100.68 MPa compressive strength, and IWP TPMS has 99.57 MPa, and uniform Schwarz D has 33.94 MPa, whereas IWP TPMS shows 31.82 compressive strength. This suggests that Schwarz D TPMS, in both uniform and graded forms, possesses the best mechanical properties, making it a promising candidate for applications demanding high strength and resilience. IWP TPMS structure also shows greater mean tensile and mean compressive strength in all cases following Schwarz D TPMS. The deformation behaviour of Schwarz P matches well with conventional lattices as per the data from stress-strain curve showing the typical compression property were an elastic compression region, a plateau region, and a densification region is observed. This study contributes to the growing interest in TPMS as a framework for designing scaffolds, leveraging their ability to mimic complex biological geometries. The successful additive manufacturing process using biomedical graded material further supports their viability in biomedical applications.

## 5. References

- [1] Zhang L et al. 2020 Tailored mechanical response and mass transport characteristic of selective laser melted porous metallic biomaterials for bone scaffolds, *Acta Biomater.* **112**, 298-315.
- [2] Collins M N et al. 2021 Scaffold fabrication technologies and structure/function properties in bone tissue engineering, *Adv. Funct. Mater.* **31**(21), 2010609.
- [3] Langer R and Vacanti J P 1993 Tissue engineering. *Science*, **260**(5110), 920-926.
- [4] Yu J, Xia H, and Ni Q Q 2018 A three-dimensional porous hydroxyapatite nanocomposite scaffold with shape memory effect for bone tissue engineering, *J. Mater. Sci.* **53**(7), 4734-4744.
- [5] Xiong J et al. 2015 Advanced micro-lattice materials, *Adv. Eng. Mater.* **17**(9), 1253-1264.
- [6] Zhang J et al. 2022 Design of a biomimetic graded TPMS scaffold with quantitatively adjustable pore size, *Mater. Des.* **218**, 110665.
- [7] Yan C et al. 2015 Ti-6Al-4V triply periodic minimal surface structures for bone implants fabricated via selective laser melting, *J. Mech. Behav. Biomed. Mater.* **51**, 61-73.
- [8] Al-Ketan O et al. 2020 Functionally graded and multi-morphology sheet TPMS lattices: Design, manufacturing, and mechanical properties, *J. Mech. Behav. Biomed. Mater.* **102**, 103520.
- [9] Santiago R et al. 2023 Modelling and optimisation of TPMS-based lattices subjected to high strain-rate impact loadings, *Int. J. Impact Eng.* **177**, 104592.
- [10] Dong Z and Zhao X 2021 Application of TPMS structure in bone regeneration, *Eng. Regener.* **2**, 154-162.
- [11] Novak N et al. 2021 Development of novel hybrid TPMS cellular lattices and their mechanical characterisation, *J. Mater. Res. Technol.* **15**, 1318-1329.
- [12] Blanquer S B and Grijpma D W 2021 Triply Periodic Minimal Surfaces (TPMS) for the Generation of Porous Architectures Using Stereolithography, *Computer-Aided Tissue Engineering: Methods and Protocols*, 19-30.
- [13] Loh Q L and Choong C 2013 Three-dimensional scaffolds for tissue engineering applications: role of porosity and pore size.
- [14] Verma R et al. 2022 Design and analysis of biomedical scaffolds using TPMS-based porous structures inspired from additive manufacturing, *Coatings*, **12**(6), 839.
- [15] Ning L and Chen X 2017 A brief review of extrusion-based tissue scaffold bio-printing, *Biotechnol. J.* **12**(8), 1600671.
- [16] Nguyen T L et al. 2011 A novel manufacturing route for fabrication of topologically-ordered porous magnesium scaffolds, *Adv. Eng. Mater.* **13**(9), 872-881.
- [17] Huang Y et al. 2017 3D bioprinting and the current applications in tissue engineering, *Biotechnol. J.* **12**(8), 1600734.
- [18] Yusong P, Qianqian S and Yan C 2013 Fabrication and characterisation of functional gradient hydroxyapatite reinforced poly (ether ether ketone) biocomposites, *Micro Nano Lett.* **8**(7), 357-361.
- [19] An J et al. 2015 Design and 3D printing of scaffolds and tissues, *Engineering*, **1**(2), 261-268.
- [20] Lu Y et al. 2020 Quantifying the discrepancies in the geometric and mechanical properties of the theoretically designed and additively manufactured scaffolds, *J. Mech. Behav. Biomed. Mater.* **112**, 104080.
- [21] Li Y et al. 2018 Additively manufactured biodegradable porous iron. *Acta Biomater.* **77**, 380-393.
- [22] Abou-Ali A M, Lee D W and Abu Al-Rub R.K 2022 On the Effect of Lattice Topology on Mechanical Properties of SLS Additively Manufactured Sheet-, Ligament, and Strut-Based Polymeric Metamaterials, *Polymers*, **14**(21), 4583.
- [23] Sankineni R and Ravi Kumar Y 2022 Evaluation of energy absorption capabilities and mechanical properties in FDM printed PLA TPMS structures. Proceedings of the Institution of Mechanical Engineers, Part C, *J. Mech. Eng. Sci.* **236**(7), 3558-3577.
- [24] Yang C et al 2023 Preparation and thermal insulation properties of TPMS 3Y-TZP ceramics using DLP 3D printing technology, *J. Mater. Sci.*, 1-16.

- [25] M Li et al. 2023 Bioadaptable bioactive glass- $\beta$ -tricalcium phosphate scaffolds with TPMS-gyroid structure by stereolithography for bone regeneration. *Journal of Materials Science & Technology*, **155**, 54-65.
- [26] Melchels F P, Feijen J and Grijpma D W 2010 A review on stereolithography and its applications in biomedical engineering. *Biomaterials*, **31**(24), 6121-6130.
- [27] Sun J, Binner J and Bai J 2019 Effect of surface treatment on the dispersion of nano zirconia particles in non-aqueous suspensions for stereolithography, *J. Eur. Ceram. Soc.* **39**(4), 1660-1667.
- [28] Yu S, Sun J and Bai J 2019 Investigation of functionally graded TPMS structures fabricated by additive manufacturing, *Mater. Des.* **182**, 108021.
- [29] Chouhan G et al 2023 Identification of Surface Defects on an SLA-Printed Gyroid Lattice Structure. in *International Conference on Research into Design*. Springer.
- [30] Biomed Clear resin safety data sheet. [cited 2023, 06.10]; Available from: <https://formlabs-media.formlabs.com/datasheets/2001424-SDS-ENUS-0.pdf>.
- [31] Austermann J et al. 2019 Fiber-reinforced composite sandwich structures by co-curing with additive manufactured epoxy lattices, *J. Compos. Sci.* **3**(2), 53.